IEEE Access
Multidisciplinary ⋮ Rapid Review ⋮ Open Access Journal

Received November 26, 2020, accepted December 31, 2020, date of publication January 12, 2021, date of current version January 27, 2021.

Digital Object Identifier 10.1109/ACCESS.2021.3051095

Infrared Thermal Images Classification for Pressure Injury Prevention Incorporating the Convolutional Neural Networks

YU WANG[1], XIAOQIONG JIANG[2], KANGYUAN YU[3], FUQIAN SHI[4], (Senior Member, IEEE), LONGJIANG QIN[1], HUI ZHOU[1], AND FUMAN CAI[2]

[1]The First Affiliated Hospital, Wenzhou Medical University, Wenzhou 325025, China
[2]College of Nursing, Wenzhou Medical University, Wenzhou 325025, China
[3]College of Optometry and Biomedical Engineering, Wenzhou Medical University, Wenzhou 325025, China
[4]Rutgers Cancer Institute of New Jersey, New Brunswick, NJ 08903, USA

Corresponding author: Fuman Cai (cfm@wmu.edu.cn)

This work was supported by the Basic Public Welfare Research Project of Zhejiang Province in 2021 under Grant LGF21H110001.

ABSTRACT Hospital-acquired pressure injury is difficult to identify in the early stage, accompanied with increased morbidity but considered to be preventable. For helping the nurses to monitor the status of the patients' skin, the infrared thermal imaging and the convolutional neural networks were integrated to identify and prevent pressure injury. In the first stage, infrared thermal images were shoot and labelled with the normal group and the pressure injury group by the clinical nurses. In the second stage, the convolutional neural networks and two machine learning algorithms, the random forest and the support vector machine, were applied to classify these two classes of the collected images. The classification model was trained on 164 images and was tested on the special image dataset consisted of 82 infrared thermal images of 1 day before pressure injury. Gray level co-occurrence matrix was utilized to extract the texture features of the infrared thermal images and we chose the pearson correlation coefficient and the Chi square test as the feature selection methods. The classification accuracy of the proposed convolutional neural networks model was 95.2% and the area under curve was 0.98. Moreover, the classification results from the test dataset were conformed to the experience of the experts. After feature selection, variance and entropy were proved to the best distinguishable features. Finally, we concluded that combining the infrared thermal imaging and convolutional neural networks could contribute to the prevention of pressure injury. This measure should be performed in high-risk populations to reduce the incidence of pressure injury.

INDEX TERMS Convolutional neural networks, thermal image, pressure injury.

I. INTRODUCTION

Pressure injury (PI), formerly known as Pressure ulcer (PU), is a local injury to the skin and soft tissue located at the bulge, medical or other instruments, and can be expressed as intact skin or openness ulcer, may be accompanied with pain [1]. Data show [2] the current PI prevalence rate of inpatients is 1.4%-120%, accompany with the PI prevalence rate was increasing year by year in the past ten years. PI has become a global health problem. It decreases health-related quality of life and is associated with fatal septic infections and higher mortality. Patients with PI have prolonged hospitalization and increased hospital costs. The rapid development and long treatment cycle of PI have brought huge economic burdens to society, medical institutions and families. Researches show that tissue damage in an area of intact skin has been penetrated from the deep to the surface within 48 hours, within 7 to 10 days for further deterioration into a necrotic. PI progresses rapidly without interventions. Thus, early detection and prevention is the only way to reduce the incidence of PI. However, there are some difficulties in clinical care carrying out the PI precaution. For one thing, the present clinical application of risk assessment scales are unable to achieve an objective and accurate assessment for early detection of the risk of pressure injury [3]. For another thing, the judgment of PI mainly depends on the evaluators' perception of vision

The associate editor coordinating the review of this manuscript and approving it for publication was Jeon Gwanggil.

and touch on spot. But inflammatory and apoptotic (necrotic) changed in the epidermal and dermal layers can precede surface changes by 3 to 10 days, hence the hysteresis of subjective judgment would lead to misunderstandings in early detection of pressure injury [4].

Currently, Infrared thermal imaging technology is the best way to solve this problem, which takes advantage of receiving infrared radiation from some parts of the scene itself. In the early stage of PI, metabolic abnormalities are caused by partial or complete occlusion of capillaries at the compression site that destroys the local thermal radiation balance, which can be recognized clearly in infrared thermal images [5] and affect the temperature of the lesion area [6]. Prior studies have noted the practicality of infrared thermal imaging in prevention of skin damage and underlying tissues. Stephanie L *et al.* [7] employed thermal imaging conjunction with image processing to monitor a patient's risk of PI during 112 days, reporting the temperature changes in patient's heels and malleolus over time. Harvey N *et al*. [8] assessed sacral skin temperature by thermal image and concluded the connection between the risk of PI (or vascular disease) and the certain temperature. And for detecting the underlying mechanisms of skin thermal damage and the optimization of clinical thermal therapies, it is believed that infrared thermal imaging technology could provide more information than biopsy and tissue histology [9]. Unfortunately, for the infrared thermal imaging, the mistakes cannot be avoided with the problems from the image quality, diagnostic experience, or shooting equipment. In order to assist doctors and nurses to better identify the patients' skin status and obtain more diagnostic information by the infrared thermal image, deep learning represented by Convolutional Neural Networks (CNN), an approach prevalent in Computer Vision and Pattern Recognition (CVPR), can be a better solution [10]. For instance, T. Jakubowska *et al.* [11] developed a breast cancer classification system based on nonlinear artificial neural network to distinguish healthy and pathological cases in infrared thermal images. The most discriminative features based on wavelet transformation in breast tumor images were obtained. Roslidar *et al*. [12] have introduced the application of CNN in the breast cancer based on thermal images, providing the summary of the current work on thermal images and an overview of the availability of breast thermal images. Juan Zuluaga-Gomez *et al*. [13] proposed a CNN hyperparameters fine-tuning optimization algorithm, identifying the breast cancer through infrared thermal imaging and the classification accuracy is 92%. Several medical research of pressure ulcers applying CNN have already been probed, but the study objects focus on PI visible images [14] which is unable to prevent early PI. While WenXue Tan [15] proposed a CNN classification model based on lesion thermal images for early warning. He summarized a self-adaptive momentum rule to update CNN parameters and the recognition accuracy is up to 96%.

Nevertheless, CNN has been prevalent in the thermal image classification task, enlightening us to apply it for the early prevention of pressure injuries. For assisting the nurses, this research shed new light on PI prevention applying infrared thermography and CNN. For the experienced nurses, the total time to complete the image acquisition and the image processing was about four to five minutes, which meeting the requirements of real-time observation. With the 4-months project, over three thousand infrared thermal images were collected and analyzed through the infrared thermal imager FLIR PRO ONE and its software support. However, only 82 patients occurred PI during hospitalization, hence our PI image dataset was small. With the original image dataset which has too little samples to train the deep learning model, it is indispensable to employ data augmentation to overcome the data insufficiency and data unbalance. After image processing mainly including image resizing and data augmentation, we proposed the PI predictive model based on collected images and CNN. In addition, to evaluate the performance of the obtained CNN model, we applied two of the machine learning algorithms to build the predict model as well. Support vector machine (SVM) and random forest (RF) are two classic and powerful algorithms to deal with the classification task of the small dataset. All the training process were employed 4-fold cross validation to test the classification results. In this procedure, Gray level co-occurrence matrix (GLCM) was used to extract the original image texture features like variance, entropy, and so on. Two methods of feature selection were also involved to assess the importance of the extracted features. Finally, comparing with other two predictive models in terms of the classification accuracy and the receiver operating characteristic curve (ROC), the performance of the CNN model was the most competitive, which were 95.2%. The main contributions of this article could be summarized in the following points: firstly, nurses can assess patients' skin condition more reliably contrasting with the traditional approaches; secondly, CNN was employed in the PI thermal image classification at first time and an elementary and reliable CNN model was attained with the limited dataset.

The rest of this article is organized as follows: Section 2 presents the main methods used in this article. The experimental details are described in Section 3. And Section 4 discusses the results concretely. Section 5 summarizes the concluding remarks and our future works of PI.

II. METHODS

A. CONVOLUTIONAL NEURAL NETWORKS

CNN, a multi-layer and non-fully-connected artificial neural network, is characteristic of convolution algorithm and successively separated into the convolutional layers, the pooling layers, the fully-connected layers, and the output layers. Two computation processes including forward propagation process and back propagation process are underwent in the whole deep learning algorithm. Two critical and classical CNN architectures are referred in our study, which are Le-Net [36], AlexNet [28], and VGGNet [29]. AlexNet has 5 convolutional layers, 3 pooling layers and 3 fully-connected layers

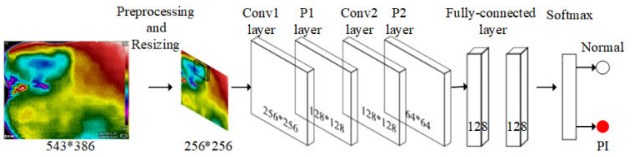

FIGURE 1. The proposed CNN architecture for the PI classification.

while VGGNet is much deeper, 11 to 16 layers, with fixed and small kernels in each convolutional layer.

The CNN architecture of this work is shown in FIGURE 1, assembling by two convolutional layers (Conv1 and Conv2), two pooling layers (P1 and P2), two fully-connected layers, and the softmax [16] classifier as the output layer.

In the two convolutional layers, the features of the infrared thermal image are extracted and analyzed by convolution computation. The equation is as follows:

$$Y(i,j) = X(i,j)^* H(i,j) \times \{i = 0, 1, \ldots, I; j = 0, 1, \ldots, J; imagesize \in [I, J]\} \quad (1)$$

where $Y(i,j)$ represents the output results of convolution computation between the input images and the convolution kernels, which transferring the three-channel RGB images into two-dimension feature map with given convolution kernels. And for the activation function, rectified linear unit (ReLU) [17] is chosen to complete the initialization of each convolutional layer. After convolution computation, the number of the output features is too considerable to exploit, therefore, another pooling layer have to be deployed to reduce the characteristic dimension. The max-pooling algorithm that is to compute the maximum values from the obtained feature map is used in this work. And for the softmax classifier, the function is:

$$P = \frac{exp(vector_c)}{\sum_{i=1}^{C} exp(vector_i)} \quad (2)$$

where P points the probability that the computed feature vector ($vector_c$) belongs to the class C. And the loss of the P is defined as below:

$$E = -\sum_{c=1}^{C} qlogP \quad (3)$$

where E represents the cross-entropy loss that assesses the performance of the training process, in which the neural networks are trained to make the output $vector_c$ close to its correct output vector from q. The q means the correct class of $vector_c$.

B. DATA AUGMENTATION

Affine transformation as the method of image augmentation is a critical and prevalent method of computer image processing in the field of image recognition exploiting artificial intelligence. Four types of data generation are chosen. Image rotation and image dilation are the main data generation approach in this article. Other methods are flip including horizontal and vertical, and normalized noises which are salt-and -pepper noise and Gaussian noise [18].

C. MACHINE LEARNING TECHNIQUES USED TEXTURE FEATURES

1) GRAY LEVEL CO-OCCURRENCE MATRIX

Gray level co-occurrence matrix (GLCM) is a join probability matrix to describe the probability of the gray value from each pixel of image, obtained by statistically computing the spatial relationship of two pixels keeping a certain distance on the image based on gray level histogram [19].

$$F(a,b|d,q) = \sum_{a=0}^{L-1}\sum_{b=0}^{L-1}((x,y)|f(x,y) = a, f(x+dx, y+dy) = b) \quad (4)$$

where (a,b) are the image pixel pairs with the distance d and the angle θ equal to 0°, 45°, 90°, and 135°. And L is the maximal gray level value number of an image sized N^*N. Thus, $F(a,b|d,\theta)$ is defined that the emergence probability of the certain pair pixels which locate in the image, shown as $(a,b)|a = f(x,y)\&b = f(x+dx, y+dy)$. Texture features extracted from the GLCM like contrast, correlation, dissimilarity, variance, and entropy [20] are employed. In the infrared thermal image, the temperature changes of the objects in the scene are collectively reflected, and the gray level distribution is concentrated, the range is narrow. Correspondingly, texture details are not rich enough. Hence, the chosen texture features should fully represent the gray level distribution of the image and reflect the gray correlation between the different regions of the image.

$$Contrast = \sum_{a=0}^{L-1}\sum_{b=0}^{L-1} F^*(a,b)|a-b|^2$$

$$(F^*(a,b) = normalizeF(a,b)) \quad (5)$$

$$Correlation = \frac{\sum_{a=0}^{L-1}\sum_{b=0}^{L-1}(a-u_1)(b-u_2)F^*(a,b)}{\sqrt{s_1 s_2}} \quad (6)$$

$$u_1 = \sum_{a=0}^{L-1}\sum_{b=0}^{L-1} aF_d^*(a,b) \quad (7)$$

$$u_2 = \sum_{a=0}^{L-1}\sum_{b=0}^{L-1} bF_d^*(a,b) \quad (8)$$

$$s_1 = \sum_{a=0}^{L-1}\sum_{b=0}^{L-1} (a-u_1)^2 F_d^*(a,b) \quad (9)$$

$$s_2 = \sum_{a=0}^{L-1}\sum_{b=0}^{L-1} (b-u_2)^2 F_d^*(a,b) \quad (10)$$

$$Dissimilarity = \sum_{a=0}^{L-1}\sum_{b=0}^{L-1} F^*(a,b)|a-b| \quad (11)$$

$$Variance = \sum_{a=0}^{L-1}\sum_{b=0}^{L-1} F^*(a,b) \times (a-Mean)^2 \quad (12)$$

$$Mean = \sum_{i=0}^{L-1}\sum_{j=0}^{L-1} F^*(a,b) \times a \tag{13}$$

$$Entropy = -\sum_{a=0}^{L-1}\sum_{b=0}^{L-1} F^*(a,b) \ln F^*(a,b) \tag{14}$$

2) SUPPORT VECTOR MACHINE AND RANDOM FOREST

Support vector machine (SVM) [21] as a supervised learning technique that prefers to solve the two-class classification problems whether are from linear or non-linear data tasks. Through creating a hyperplane in a high-dimensional space, SVM seeks the best optimal parameters to determine the best hyperplane which divides the data into different classes with the maximize distance between two classes. Several kernel functions (for instance, linear, polynomial, and radial basis) can estimate the margins and the kernel, polynomial, is the commonest choice.

And random forest (RF) [22] is a concept of ensemble learning, made by various decision trees in the training process. For RF, the output class label is determined by the mode of the class output by the individual tree. Numerous decision trees can handle the different feature subsets and produce independent results, and with optimal split times, RF can tackle outliers and noise in the dataset. Another advantage of RF is less susceptible to overfitting, which is attractive to use with the small dataset.

D. FEATURE SELECTION AND EVALUATION

Feature selection is an efficient approach to shrink feature dimensions through choosing the effective features from the original feature dataset in image processing. And the more valuable characteristics could be selected in this process. Pearson correlation coefficient[23] and Chi square test[24] are two correlation criteria in this article considering the applicability and simplicity of our dataset.

The classification performance is evaluated by the receiver operating characteristic curve (ROC) and the area under curve (AUC) [25]. and other metrics are accuracy, specificity, sensitivity, which are shown as follows:

$$Accuracy = \frac{TP + TN}{S} \tag{15}$$

Accuracy is the kernel evaluation metric and describes the total number of the true positive cases and true negative cases in the whole cases (S). In the test results, TP means that the predict label of the case is consistent with the actual label and TN means that the predict label of the case is opposite with the actual label. Thus, there are also FN and FP.

$$Specificity = \frac{TN}{TN + FP} \tag{16}$$

Specificity is computed as TN divided by the total number of the cases labeled with negative, which evaluates the performance of the model towards to the negative cases. And specificity is called TNR as well, meaning the true negative rate.

$$Sensitivity = \frac{TP}{TP + FN} \tag{17}$$

Contrary to the specificity, sensitivity evaluates the performance of the model about the positive cases, meaning the true positive rate (TPR).

III. EXPERIMENTAL DETAILS

A. DATASETS

From August 2018 to April 2019, 349 patients, who were followed up continuously for 10 days, from some departments of intensive care unit (ICU) were selected in the first affiliated hospital of Wenzhou Medical University.

The infrared device used for the acquisition of skin thermal images is from the FLIR ONE PRO [26], with which an optical camera (visible light resolution up to 1440 * 1080 dpi) and an infrared camera (thermal resolution up to 160 * 120 dpi) supported with the software provided by FLIR ONE. And the temperature resolution is 0.1 °C with a temperature range of −20 °C to 400 °C. The manual of the device could learn from [37].

Apart from the unqualified samples, over three thousand infrared thermal images of sacral region were acquired from 349 cases. With an incidence rate of pressure injury of 23.5% which was accord with the study [27], there were 82 cases in PI in the whole process. Thus, there were 82 PI infrared thermal images. And in order to the data balance, another 82 normal infrared thermal images were selected from all shot images. In addition, all abnormal ones belonged to status 1 of PI merely, making the warning values of tissue damage more practical. Especially, because all the images of patients' skin condition were collected for 10 consecutive days, the images of the 82 patients 1 day before the pressure ulcer were recorded as well. For the prevention of the PI, it is significant to explore the patient's skin condition before the PI occurring. Therefore, 82 infrared thermal images of 1 day before patient occurring PI were marked as the test dataset to verify our framework. However, the 82 images in test dataset were not sure to label with PI, thus, we hypothesized that all of them were PI. In this way, there were two image datasets in this article, which were the train dataset (82 PI infrared thermal images and 82 normal infrared thermal images) and the test dataset (82 infrared thermal images of 1 day before PI).

The details of thermal image acquisition were as follow:

The preparation of environment mainly included temperature and humidity inside ward which were 22°C to 26 °C and 50% to 60%, respectively.

For the preparation of patients, participants were prohibited to have physical therapy. Then, participants were asked not to take any activities likewise move, eat, wash, and bath within 30 minutes before measurement. During the shooting process, patients need to stay in bed with the 90 degrees lateral position lasts 4 minutes, exposing the area required for the sacral region and lower back completely. Meanwhile,

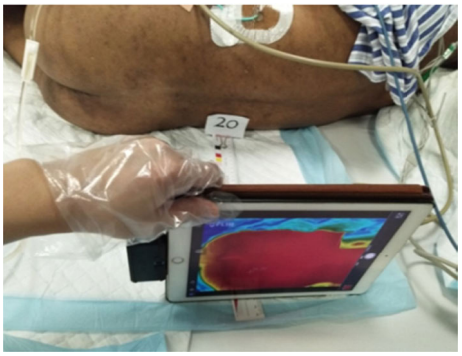

FIGURE 2. Process for the PI thermal image collection through infrared thermal camera and tablet personal computer.

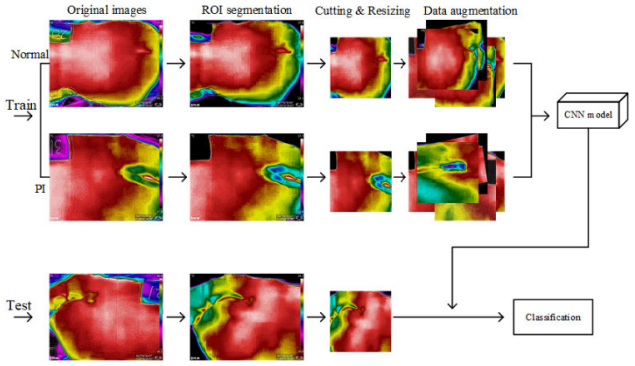

FIGURE 3. Pipeline of the proposed CNN architecture based on classifier.

the device kept at 30cm from the sacral area when taking the thermal images. Make sure that the infrared thermal imager was parallel to the body, it was perpendicular to the bed surface, and the lens was at the same height as sacrum.

B. IMAGE PREPROCESSING

In imaging procedure, all the obtained thermal images are 546*386 pixels, and each one has a related file containing temperature value of each pixel.

There are two main steps in the image preprocessing which are the ROI segmentation and data augmentation. For ROI segmentation, nurses experienced and mastered in infrared thermal image software could separate the ROI from the original thermal image easily and quickly with FLIR software and label the original thermal image with normal or pressure injury. And for the data augmentation, we expanded the raw dataset 14 times through rotating in 5 different angles (60°, 90°, 120°, 180°, 270°); flipping in horizontal and vertical; dilating 5 different seeds in the same ROI; and adding gaussian noise and salt pepper noise into the raw images with parameters (in the Gaussian noise, the mean was 0.1 and the variance was 0.05; in the salt & pepper noise, the parameter was 0.03). Thereby, the number of the original images increased from 164 to 2296.

C. DETAILS OF CNN LAYERS AND TRAINING

Each image of size 546*386 is resized to 256*256 after image preprocessing and data normalization. In the first convolutional layer (Conv1 layer), 16 convolutional kernels of size 3*3 are applied to work with the input images (256*256). Successively, the output (the images still size in 256*256) of Conv1 layer will be fed into the first pooling layer (P1 layer) that is component of one convolutional kernel sized in 3*3. And the second convolutional layer (Conv2 layer) and the second pooling layer (P2 layer) are same as the first ones. However, the input patches in Conv2 layer and P2 layer are which is exactly the results of the first convolutional layer. The activation function used in two Conv layers and two pooling layers is ReLU. Both of the fully-connected layers have 128 neurons, transforming the output features computed from

TABLE 1. The Setting Parameters in Training Procedure

Layers	Output	Conv Kernel	Stride	Padding	Dropout ratio
Input images	(3,256*256)				
Conv1	(3,256*256)	(16,3*3)	1	1	
P1	(3,128*128)	(1,3*3)	2	1	
Conv2	(3,128*128)	(16,3*3)	1	1	
P2	(3,64*64)	(1,3*3)	2	1	
FC1	128				0.4
FC2	128				0.4
SoftMax	2				

Conv2 layer and P2 layer into vectors correspond to the two targeted classes, normal and PI. And for supervising the fine-tuning during back propagation, ''AdamOptimizer'' is used as well [28]. For training the model using CNN, 2296 infrared thermal images after preprocessing were separated into two groups, which were test group including 20% and the train group including 80%.

Tensorflow3.0 and MATLAB 2016A work on the development environment, windows10. And the framework of the PI infrared thermal image classification is illustrated in FIGURE 3. Steps of the whole image processing are as follows:

1) Select and label the skin infrared thermal images by nurses and doctors;
2) Segment the ROI from the original infrared thermal images;
3) Resize the input images into 256*256;
4) Apply data augmentation to expand the original image dataset; separate the augmented dataset into train dataset and test dataset by assigning the images randomly;
5) Train the CNN model and evaluate the CNN model.

TABLE 1 illustrates the specific setups of the proposed CNN model and the significant setups of training parameters. ''Stride'' and ''Padding'' (the strategy is ''SAME'') determine the size of the feature maps in each layer. And during an unbroken training process which needs around from 3,600 seconds to 4,000 seconds, the basic learning rate is 0.001, the batch size is 64, and the epoch is 751.

D. IMPLEMENTATION AND PARAMETERS OF SVM AND RF CLASSIFIERS

After image preprocessing, 5 texture features from all the infrared thermal images were extracted using GLCM. And the strategy of the dataset separation is same as the CNN pipeline, 20% for test and 80% for train.

The implementation of SVM was performed using LIBSVM [29] package. The two most important parameters are the optimum parameter of cost and the kernel width. And with the polynomial kernel, automatic optimization in 4-fold cross validation was employed to find the best parameters according to a stride of 0.5 and ranging from -10 to 10. Eventually, the best parameter of cost was 1024 and the best parameter of the kernel width was 724.0773. And the implementation of RF was used the python package ''scikit-learn''. Some default parameters of the RF classifier set in our task were derived from [30]. The main parameters changed were the number of trees which was 15 and the number of random sampling regions was 10. All texture features based on GLCM were taken as input features.

IV. RESULTS AND DISCUSSION

After the whole study, we have proposed a novel solution for the PI problem that is focus on the diagnosis and prevention. The proposed method integrates infrared thermal imaging and artificial intelligence to assess skin condition of critically ill patients, suggesting a new assessment as a complementary index to improve the level of care for critically ill patients. Firstly, several significant discoveries have been found through comparing the differences between the normal skin infrared thermal images and the pressure injury infrared thermal images. Recent research demonstrates that different color gradations represents different temperatures in thermal image: red for hot zone, yellow for warm zone, green for cool zone, blue for cold zone, and purple for supercool zone [31]. Generally, as blood perfusion and tissue metabolism are constant at one anatomical region, implying color gradation distribution should be uniform. As adipose tissue generally does not transmit heat, the subcutaneous fat-rich parts have lower skin temperatures (such as the hip) [32]. Therefore, the hip area appears as yellow warm zone compared to red hot zone of sacrum in thermal images. When the injury occurs, the red zone of sacrum presents a yellow abnormal color gradation. Moreover, the whole change process takes place before the skin abnormality is recognized by the naked eye. As tissue damage aggravate, yellow-green color gradation appears, finally changing into a green abnormal color gradation. Correspondingly, the subjectivity and indirectness of risk assessment scales hinder nurses to identify local skin changes sensitively and timely. And it is easy for clinical nurses to become complacent over time for scale score, which results in poor triggers for taking preventive measure.

Secondly, although using GLCM could obtain several texture features from images, entropy and variance are the most distinguishable features to the infrared thermal images [8], [33], which is also accord from FIGURE 5. FIGURE 5 presents the mean of the 5 texture features extracted from the normal dataset, the PI dataset, and the test dataset. Generally, contrast, correlation, dissimilarity, and entropy can describe the image sufficiently, but in the infrared thermal images, mainly because of the image quality and image content, the difference of the three features is not conspicuous. FIGURE 5 also describes that the entropy from PI images is the highest score, suggesting the PI images are more complex.

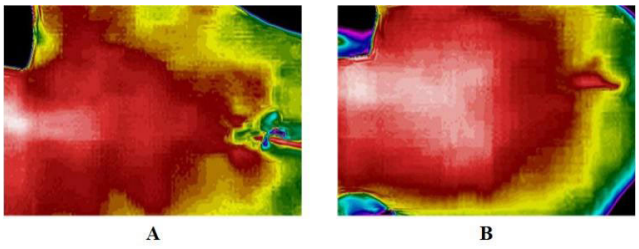

FIGURE 4. Two samples of the sacral region infrared thermal images: A is the pressure injury in status 1, appearing yellow or green abnormal color gradation in the top region of sacrum; and B is a normal infrared thermal image.

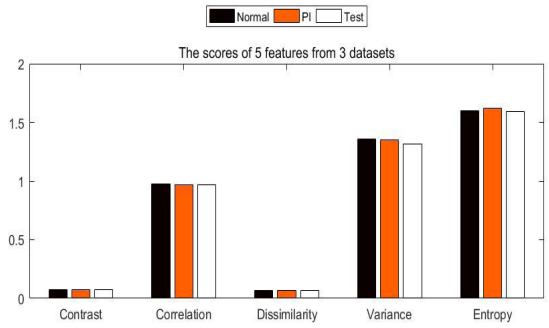

FIGURE 5. The scores of the 5 texture features extracted from 3 datasets using GLCM.

Through the feature selection step, the conclusion that the entropy and variance are the most efficient texture features for the infrared thermal images has been verified again. In TABLE 2, the texture features are the image data applied in the classification model. Variance and entropy value 0.092 and 0.084 using pearson coefficient correlation, respectively. Both of the two features are lower than other three features, pointing out the variance and entropy are more efficient. And for Chi square, the higher the score is, the stronger the connection between the features and images. Another index RF value is come from the process of training model in RF algorithm, which indicates that except variance or entropy, dissimilarity is also an important feature for building the classification model. However, other two feature selection methods do not denote that, thus, we merely concluded that the dissimilarity was more important than contrast or correlation in building our models using random forest algorithm.

FIGURE 6 shows the ROC curves of the three classification models building by the SVM algorithm, the RF

TABLE 2. The Scores of the 5 Texture Features Using Random Forest Values, Pearson Correlation Coefficient, and Chi Square

Features	RF value	Pearson correlation coefficient	Chi square
Contrast	0.188	0.708	0.774
Correlation	0.185	0.662	0.685
Dissimilarity	0.208	0.731	0.765
Entropy	0.203	0.084	0.968
Variance	0.216	0.092	0.834

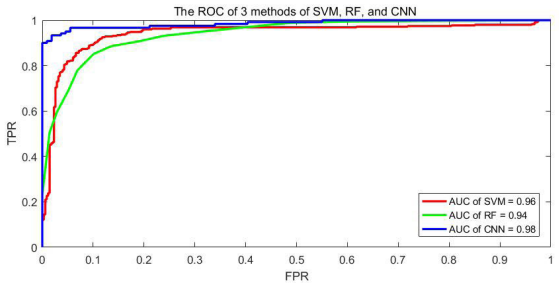

FIGURE 6. The ROC of the three algorithms.

TABLE 3. The Details of the 3 Classification Models

	CNN	SVM	RF
Specificity	93.58%	89.08%	86.49%
Sensitivity	96.67%	90.52%	88.51%
Accuracy	95.2%	89.8%	87.5%
AUC	0.98	0.96	0.94

algorithm, and the proposed CNN framework. According to the ROC curves, the CNN model has the best classification performance and the corresponding AUC is 0.98. Despite the two traditional methods, SVM and RF, have an inferior classification results, the AUC of the two model is still higher than the existing models [34] of the infrared thermal images. In addition, although comparing other deep CNN model [14], our CNN framework has a more simple and concise structure, the computational efficiency of the proposed CNN method is still lower than other two machine learning methods which just need 1200 seconds to 1500 seconds.

TABLE 3 presents the specificity, sensitivity, accuracy, and AUC of the three classification models. The details of the proposed CNN model show a higher performance than other two machine learning methods. And as compared with other CNN applications in thermal images [11], the accuracy of 95.2% is also better than the existing CNN models. In the three models, the specificities are all lower than the sensitivities, suggesting that the classification models have a stronger ability to identify positive cases. And in general, with the same five texture features, the model using SVM methods is equal to the model of RF. Both of our two methods overperform some models applying traditional machine learning methods like artificial neural network [35] (our classification accuracy is 86% to 89%, while other systems scored around 80%), indicating the advantages of our works.

However, when we used the test dataset including 82 thermal images of 1 day before PI to test the obtained three

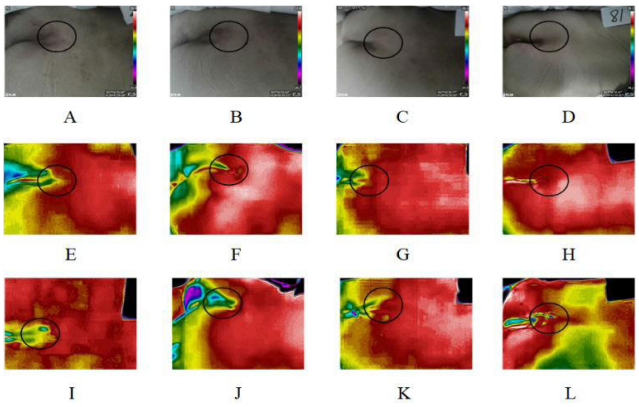

FIGURE 7. The first row (A to D) are the vision images of 1 day before PI; the second row (E to H) are the thermal images of 1 day before PI; and the third row (I to L) are the thermal images of the day of PI occurred. The black circle area represents the ROI.

models, the CNN was still the most competitive, but the model using the RF method was obviously superior to the model of SVM, which implies the ensemble learning algorithm has a great potential as well. In test dataset, most cases were not diagnosed even by experienced nurses, but the CNN model distinguished 66 PI infrared thermal images, which assisted nurses to assess the patient's skin condition.

Some examples of the test dataset are presented in FIGURE 7. Four examples displayed in FIGURE 7 which were in doubt in the labelling process, because we could not diagnose the patient's skin condition positively by the observing situation on site or even through the infrared thermal imaging. The first row of FIGURE 7 acquired through the infrared thermal imaging accordingly are the visible images of 1 day before PI, but only the FIGURE 7A and FIGURE 7B could be diagnosed by nurses. On the contrary, the second row of the FIGURE 7 could describe the patient's skin condition clearly, which are also the best examples that can represent the dataset. While encountering these cases before PI occurred, the professional nurses will hesitate to determine whether to take protective measures or not only with the naked eye skin observation. However, PI just occurred after several hours, and this change was shown from the third row of the FIGURE 7 obviously, compared with the infrared thermal imaging of 1 day before PI. We can point out that the abnormal change (appeared yellow or green zone) of sacral region in FIGURE 7E to FIGURE 7H is early warning signal of skin injury, which were verify the reliability of early warning further when PI occurred with the color zone turned colder. Therefore, we made a hypothesis that how deep learning works in this application may be based on it. Eventually, 66 infrared thermal imaging samples of 1 day before PI in in this dataset were identified as PI by CNN model, which is also supported by the nurses.

Overall, from FIGURE 7 and TABLE 4, the infrared thermal images and the classification results of the three models indicate the dilemma of the infrared thermography

TABLE 4. The Classification Results of the 3 Classification Models on Test Dataset

	CNN	SVM	RF
Test Accurate numbers	66	50	59

and the deficiency of the artificial intelligence applied to PI: acquiring images at a single point in time is not sufficient to prevent PI, neither for nursing staff nor artificial intelligence. Thereby, in order to prevent PI effectively and modify our CNN model, more thermal images of the potential areas where PI occur ought to be collected in different point-in-time. Another limitation of our work lies in the ROI segmentation process, it is still a subjective process to delete the background and other redundant information from the original infrared thermal images by manual. As a consequence, it took us a great deal of time to discuss the thresholds of some ambiguity images, especially in the dataset of the 1 day before PI occurred.

V. CONCLUSION

In this article, infrared thermal imaging technology was employed to prevent PI rather than the conventional risk assessment scales, providing more objective and directive diagnostic method. And integrating the infrared thermal imaging with the CNN, we presented a CNN model to identify the infrared thermal images. As far as we know, CNN has been applied in many different images, but when it comes to the infrared thermal image of which the gray level is more concentrated and the content is coarser, the existing CNN models should be adjusted to use. A specified CNN architecture for thermal image ought to be more concise and more convenient to train. Test results have shown that our proposed framework achieves competitive capability in the train and test datasets. And comparing with the SVM and RF, the CNN model performs better, and we also verify the more significant features for the infrared thermal images, which are variance and entropy. Promising results indicate there are great potential value in the prevention of pressure injury with exertion of infrared thermography and CNN. In future works, our project is still continuing and more PI cases will be gathered in our datasets. We will increase the number of PI thermal images to train more models with other CNN architectures for obtaining the more satisfied and reliable results.

ACKNOWLEDGMENT

The authors would like to acknowledge the participants and their families for taking part in this study and the assistance of all administrators and staff in hospital.

REFERENCES

[1] J. E. Schank, "The NPUAP meeting—This was no consensus conference," *J. Amer. College Clin. Wound Spec.*, vol. 7, nos. 1–3, pp. 19–24, Dec. 2015, doi: 10.1016/j.jccw.2016.07.001.

[2] C. VanGilder, C. Lachenbruch, C. Algrim-Boyle, and S. Meyer, "The international pressure ulcer prevalence survey: 2006-2015," *J. Wound, Ostomy Continence Nursing*, vol. 44, no. 1, pp. 20–28, 2017, doi: 10.1097/WON.0000000000000292.

[3] L. Šateková, K. Žiakov, and R. Zeleníkov, "Predictive validity of the Braden scale, Norton scale, and Waterlow scale in the Czech Republic," *Int. J. Nurs. Pract.*, vol. 23, no. 1, pp. 1–10, Nov. 2016, doi: 10.1111/ijn.12499.

[4] Z. Moore, D. Patton, S. L. Rhodes, and T. O'Connor, "Subepidermal moisture (SEM) and bioimpedance: A literature review of a novel method for early detection of pressure-induced tissue damage (pressure ulcers)," *Int. Wound J.*, vol. 14, no. 2, pp. 331–337, Apr. 2017, doi: 10.1111/iwj.12604.

[5] B. Casanova, Olga, B. Gómez, Nuria, P. Quesada, J. Ignacio, G. Gonzalez, C. Mauricio, C. O. d. Anda, R. María, S. Palmero, Rosario, N. Gómez, and Francisco, "Application of infrared thermography in diagnosing peripherally inserted central venous catheter infections in children with cancer," *Physiolog. Meas.*, vol. 40, no. 4, pp. 1–8, Apr. 2019, doi: 10.1088/1361-6579/ab031a.

[6] X. Jiang, X. Hou, N. Dong, H. Deng, Y. Wang, X. Ling, H. Guo, L. Zhang, and F. Cai, "Skin temperature and vascular attributes as early warning signs of pressure injury," *J. Tissue Viability*, vol. 29, no. 4, pp. 258–263, Nov. 2020, doi: 10.1016/j.jtv.2020.08.001.

[7] S. L. Bennett, R. Goubran, and F. Knoefel, "Long term monitoring of a pressure ulcer risk patient using thermal images," in *Proc. 39th Int. Conf. IEEE Eng. Med. Biol. Soc.*, Jeju Island, South Korea, Jul. 2017, pp. 1461–1464.

[8] H. N. Mayrovitz, P. E. Spagna, and M. C. Taylor, "Sacral skin temperature assessed by thermal imaging: Role of patient vascular attributes," *J. Wound, Ostomy Continence Nursing*, vol. 45, no. 1, pp. 17–21, 2018, doi: 10.1097/WON.0000000000000392.

[9] F. Xu, P. F. Wang, M. Lin, T. J. Lu, and E. Y. K. Ng, "Quantification and The Underlying Mechanism of Skin Thermal Damage: A Review," *J. Mech. Med. Biol.*, vol. 10, no. 3, pp. 373–400, Sep. 2010, doi: 10.1142/S0219519410003459.

[10] S. M. Anwar, M. Majid, A. Qayyum, M. Awais, M. Alnowami, and M. K. Khan, "Medical image analysis using convolutional neural networks: A review," *J. Med. Syst.*, vol. 42, no. 11, pp. 226–245, Oct. 2018, doi: 10.1007/s10916-018-1088-1.

[11] T. Jakubowska, B. Wiecek, M. Wysocki, C. Drews-Peszynski, and M. Strzelecki, "Classification of breast thermal images using artificial neural networks," in *Proc. 26th Annu. Int. Conf. IEEE Eng. Med. Biol. Soc.*, Sep. 2004, pp. 1155–1158.

[12] R. Roslidar, A. Rahman, R. Muharar, M. R. Syahputra, F. Arnia, M. Syukri, B. Pradhan, and K. Munadi, "A review on recent progress in thermal imaging and deep learning approaches for breast cancer detection," *IEEE Access*, vol. 8, pp. 116176–116194, Jun. 2020, doi: 10.1109/ACCESS.2020.3004056.

[13] J. P. Zuluaga-Gomez, Z. A. Masry, K. Benaggoune, S. Meraghni, and N. Zerhouni, "A CNN-based methodology for breast cancer diagnosis using thermal images," in *Proc. Comput. Vis. Pattern Recognit.*, Oct. 2020.

[14] B. García-Zapirain, M. Elmogy, A. El-Baz, and A. S. Elmaghraby, "Classification of pressure ulcer tissues with 3D convolutional neural network," *Med. Biol. Eng. Comput.*, vol. 56, no. 12, pp. 2245–2258, Jun. 2018, doi: 10.1007/s11517-018-1835-y.

[15] W. X. Tan, C. J. Zhao, and H. R. Wu, "CNN intelligent early warning for apple skin lesion image acquired by infrared video sensors," *High Technol. Lett.*, vol. 22, no. 1, pp. 67–74, May 2016, doi: 10.3772/j.issn.1006-6748.2016.01.010.

[16] S. Horiguchi, D. Ikami, and K. Aizawa, "Significance of softmax-based features in comparison to distance metric learning-based features," *IEEE Trans. Pattern Anal. Mach. Intell.*, vol. 42, no. 5, pp. 1279–1285, May 2020, doi: 10.1109/TPAMI.2019.2911075.

[17] A. Krizhevsky, I. Sutskever, and G. E. Hinton, "ImageNet classification with deep convolutional neural networks," in *Proc. 25th Int. Conf. Neural Inf. Process. Syst.*, New York, NY, USA, Dec. 2012, pp. 1097–1105.

[18] V. M. Kamble and K. Bhurchandi, "Noise estimation and quality assessment of Gaussian noise corrupted images," presented at the 3rd Int. Conf. Commun. Syst., Rajasthan, India, Oct. 2017.

[19] B. Chanda, B. B. Chaudhuri, and D. D. Majumder, "On image enhancement and threshold selection using the graylevel co-occurence matrix," *Pattern Recognit. Lett.*, vol. 3, no. 4, pp. 243–251, Jul. 1985, doi: 10.1016/0167-8655(85)90004-2.

[20] Y. Wang, Y. Chen, N. Yang, L. Zheng, N. Dey, A. S. Ashour, V. Rajinikanth, J. M. R. S. Tavares, and F. Shi, "Classification of mice hepatic granuloma microscopic images based on a deep convolutional neural network," *Appl. Soft Comput.*, vol. 74, pp. 40–50, Jan. 2019, doi: 10.1016/j.asoc.2018.10.006.

[21] R.-E. Fan, P.-H. Chen, and C.-J. Lin, "Working set selection using second order information for training support vector machines," *J. Mach. Learn. Res.*, vol. 6, pp. 1889–1918, Dec. 2005, doi: 10.1115/1.1898234.

[22] I. Ahmad, M. Basheri, M. J. Iqbal, and A. Rahim, "Performance comparison of support vector machine, random forest, and extreme learning machine for intrusion detection," *IEEE Access*, vol. 6, pp. 33789–33795, May 2018, doi: 10.1109/ACCESS.2018.2841987.

[23] I. Guyon and A. Elisseeff, "An introduction to variable and feature selection," *J. Mach. Learn. Res.*, vol. 3, pp. 1157–1182, Jan. 2003, doi: 10.1063/1.106515.

[24] P. Vidyullatha and D. R. Rao, "Machine learning techniques on multidimensional curve fitting data based on R-square and chi-square methods," *Int. J. Electr. Comput. Eng.*, vol. 6, no. 3, pp. 974–979, Jun. 2016, doi: 10.11591/ijece.v6i3.9155.

[25] L. E. Bantis and Z. Feng, "Comparison of two correlated ROC curves at a given specificity or sensitivity level," *Statist. Med.*, vol. 35, no. 24, pp. 4352–4367, Jun. 2016, doi: 10.1002/sim.7008.

[26] T. Kanazawa, G. Nakagami, T. Goto, H. Noguchi, M. Oe, T. Miyagaki, A. Hayashi, S. Sasaki, and H. Sanada, "Use of smartphone attached mobile thermography assessing subclinical inflammation: A pilot study," *J. Wound Care*, vol. 25, no. 4, pp. 177–182, Apr. 2016, doi: 10.12968/jowc.2016.25.4.177.

[27] M. I. González-Méndez, M. Lima-Serrano, C. Martín-Castaño, I. Alonso-Araujo, and J. S. Lima-Rodríguez, "Incidence and risk factors associated with the development of pressure ulcers in an intensive care unit," *J. Clin. Nursing*, vol. 27, nos. 5–6, pp. 1028–1037, Dec. 2017, doi: 10.1111/jocn.14091.

[28] G. Yang, J. Yang, S. Li, and J. Hu, "Modified CNN algorithm based on Dropout and ADAM optimizer," *J. Huazhong Univ. Sci. Technol.*, vol. 46, no. 7, pp. 122–127, Jul. 2018, doi: 10.13245/j.hust.180723.

[29] C.-C. Chang and C.-J. Lin, "LIBSVM: A library for support vector machines," *ACM Trans. Intell. Syst. Technol.*, vol. 2, no. 3, pp. 1–27, Apr. 2011, doi: 10.1145/1961189.1961199.

[30] R. Lahmyed, M. El Ansari, and A. Ellahyani, "A new thermal infrared and visible spectrum images-based pedestrian detection system," *Multimedia Tools Appl.*, vol. 78, no. 12, pp. 15861–15885, Jun. 2019, doi: 10.1007/s11042-018-6974-5.

[31] C.-L. Huang, Y.-W. Wu, C.-L. Hwang, Y.-S. Jong, C.-L. Chao, W.-J. Chen, Y.-T. Wu, and W.-S. Yang, "The application of infrared thermography in evaluation of patients at high risk for lower extremity peripheral arterial disease," *J. Vascular Surg.*, vol. 54, no. 4, pp. 1074–1080, Oct. 2011, doi: 10.1016/j.jvs.2011.03.287.

[32] S. García-Mayor, J. C. Morilla-Herrera, I. Lupiáñez-Pérez, S. K. Uttumchandani, Á. León Campos, M. Aranda-Gallardo, A. B. Moya-Suárez, and J. M. Morales-Asencio, "Peripheral perfusion and oxygenation in areas of risk of skin integrity impairment exposed to pressure patterns. A phase i trial (POTER Study)," *J. Adv. Nursing*, vol. 74, no. 2, pp. 465–471, Feb. 2018, doi: 10.1111/jan.13414.

[33] S. Kacmaz, E. Ercelebi, S. Zengin, and S. Cindoruk, "The use of infrared thermal imaging in the diagnosis of deep vein thrombosis," *Infr. Phys. Technol.*, vol. 86, pp. 120–129, Nov. 2017, doi: 10.1016/j.infrared.2017.09.005.

[34] A. Lashkari, F. Pak, and M. Firouzmand, "Breast thermal images classification using optimal feature selectors and classifiers," *J. Eng.*, vol. 2016, no. 7, pp. 237–248, Jul. 2016, doi: 10.1049/joe.2016.0060.

[35] H. L. Chen, S. J. Yu, Y. Xu, S. Q. Yu, J. Q. Zhang, J. Y. Zhao, P. Liu, and B. Zhu, "Artificial neural network: A method for prediction of surgery-related pressure injury in cardiovascular surgical patients," *J. Wound Ostomy Continence Nursing Off. Publication Wound Ostomy Continence Nurses Soc.*, vol. 45, no. 1, pp. 26–30, Feb. 2018, doi: 10.1097/WON.0000000000000388.

[36] Y. Lecun, L. Bottou, Y. Bengio, and P. Haffner, "Gradient-based learning applied to document recognition," *Proc. IEEE*, vol. 86, no. 11, pp. 2278–2324, Nov. 1998, doi: 10.1109/5.726791.

[37] Y. Y. Ji, W. H. Xu, D. B. Ma, and Y. Li, "Altering integral time method in temperature measurement using mid-wavelength infrared imaging system," *Appl. Mech. Mater.*, vols. 401–403, pp. 1519–1522, Sep. 2013, doi: 10.4028/www.scientific.net/AMM.401-403.1519.

YU WANG received the B.S. degree in biomedical engineering from Taishan Medical University, China, in 2016, and the master's degree in biomedical engineering from Wenzhou Medical University, China, in 2019. He is currently a Biomedical Engineer with the Department of Medical Engineering, The First Affiliated Hospital, Wenzhou Medical University. His research interests include medical image mining, infrared thermal imaging, and deep neural networks.

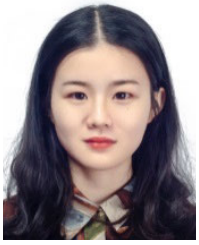

XIAOQIONG JIANG received the master's degree in nursing science from Wenzhou Medical University, China, in 2020. She is currently a Surgical Nursing Teacher with Wenzhou Medical University, where she is also with the Faculty of Nursing. She devoted herself to the research of wound and stoma care and cured the patients away from the pain of wound as a Specialist Nurse. Her research interests include the caring of wound and stoma, and the prevention and treatment of wounds.

KANGYUAN YU received the B.S. degree in biomedical engineering from Wenzhou Medical University, China, in 2018, where he is currently pursuing the master's degree in biomedical engineering with the College of Optometry and Biomedical Engineering. His research interests include biophotonics and deep neural networks.

FUQIAN SHI (Senior Member, IEEE) received the Ph.D. degree in engineering from the College of Computer Science and Technology, Zhejiang University. He was a Visiting Associate Professor with the Department of Industrial Engineering and Management System, University of Central Florida, Orlando, FL, USA, from 2012 to 2014. He is currently an Associate Professor with the Rutgers Cancer Institute of New Jersey, New Brunswick, NJ, USA. He serves more than 30 committee board memberships for international conferences. He has published more than 80 journal articles and conference proceedings. His research interests include fuzzy inference system, artificial neuro networks, and biomechanical engineering. He also serves as an Associate Editor for the *International Journal of Ambient Computing and Intelligence* (IJACI), the *International Journal of Rough Sets and Data Analysis* (IJRSDA), and a Special Issue Editor of fuzzy engineering and intelligent transportation in *Information: An International Interdisciplinary Journal*.

LONGJIANG QIN received the B.S. degree in biomedical engineering from Wenzhou Medical University, China, in 2011. He is currently a Biomedical Engineer with the Department of Medical Engineering, The First Affiliated Hospital, Wenzhou Medical University. His research interests include biomedical optics and machine learning.

HUI ZHOU received the B.S. degree in biomedical engineering from Wenzhou Medical University, China, in 2011. She is currently a Biomedical Engineer with the Department of Medical Engineering, The First Affiliated Hospital, Wenzhou Medical University. Her research interests include biomedical sensors and medical optics.

FUMAN CAI received the B.S. degree in nursing science from Zhejiang University, China, in 2000, and the master's degree in pathophysiology from Wenzhou Medical University, China, in 2006. He is currently working with the Faculty of Nursing, Wenzhou Medical University. He is an Associate Professor. His research interest includes the image system research of pressure injury risk warning. He has published ten articles in this field.